Comparison of 3D Image Reconstruction Techniques using Real Electrical Impedance Measurement Data

Stephenson, David R and Davidson, John L and Lionheart, William R.B. and Grieve, Bruce D and York, Trevor A

2005

MIMS EPrint: **2009.11**

Manchester Institute for Mathematical Sciences
School of Mathematics

The University of Manchester

Reports available from: http://eprints.maths.manchester.ac.uk/
And by contacting: The MIMS Secretary
School of Mathematics
The University of Manchester
Manchester, M13 9PL, UK

ISSN 1749-9097

Comparison of 3D Image Reconstruction Techniques using Real Electrical Impedance Measurement Data

D R Stephenson[1], J L Davidson[1], W R B Lionheart[1], B D Grieve[2], T A York[1]

[1] University of Manchester, M60 1QD, UK, t.a.york@manchester.ac.uk
[2] Syngenta Ltd, Global Specialist Tech., Huddersfield, HD2 1FF, UK, bruce.grieve@syngenta.com

ABSTRACT

The present status of electrical impedance tomography (EIT) is such that many successful laboratory based studies and pilot plant demonstrators are generating interest in developing the technology. However, while the EIT problem is inherently 3D, many studies make 2D assumptions in order to simplify the problem. Proportionately less work has been carried out on the true 3D EIT problem, outside of the mathematical development of the problem. This paper aims to provide a comparison of the performance of 3D EIT image reconstruction algorithms applied to real data, and assess whether the extra effort and complexity involved in 3D EIT is worthwhile. Measurement data are taken from a pilot-scale mixing vessel. The performance of five common EIT reconstruction algorithms is compared and the best performing algorithm for this arrangement is identified. This work is part of the ongoing efforts at Manchester to pursue the true 3D EIT problem under the EIDORS-3D framework.

Keywords EIT, Image Reconstruction, Comparison of algorithms, EIDORS 3D.

1 Introduction

Electrical impedance tomography (EIT) is an inherently 3D problem. Since Calderón proved the uniqueness of the conductivity inverse boundary value problem in 1980 (Calderón, 1980), the vast majority of work undertaken in EIT has utilised 2D measurements and reconstruction techniques in an attempt to interrogate a 3D domain. Historically, 2D assumptions were made in order to overcome electrical hardware and computational issues. Recent advances in both hardware and computational power have enabled further research into the true 3D problem. Much of the recent understanding of the mathematics involved in 3D EIT has been as a result of simulated EIT experiments (Borsic, 2002; Molinari *et al*, 2002). 2D assumptions have enabled a body of work to be undertaken since the mid 1980's within the medical, geophysical and process fields (Brown, 2001; Daily *et al* 1995; Dickin *et al* 1993). However, a survey of the literature on EIT confirms that relatively few studies within the process tomography arena have employed both 3D data collection and image reconstruction, notable exceptions include Davidson *et al* (2004) and Pinheiro (1998). The work reported in this paper aims to form a comparison of the performance of five popular image reconstruction algorithms, Linear Back-Projection, Linear Landweber, Linear Conjugate Gradients, Linear Regularised Gauss-Newton and Non-Linear Regularised Gauss-Newton. The performance of the algorithms is compared using voltage measurements taken from a pilot-scale laboratory vessel containing mains tap water, in which various phantoms were placed.

As 2D EIT has witnessed many successful applications within the process sector over the past fifteen years (Dyakowski *et al*, 2000), one could legitimately ask is the extra effort and complexity involved in 3D EIT worthwhile? The motivation for this work is to attempt to answer this question, using measurements from real experiments. The increased accuracy of 3D EIT over 2D EIT promises to offer better estimation of materials distribution within processes. This would imply that better estimation of materials distribution within processes leads to improved estimation of process parameters, and ultimately, an increased understanding of processes impacting on bottom line profitability.

2 Mathematical Setting

EIT belongs to a family of non-invasive, soft field electrical tomographic modalities. In EIT, the internal complex admittivity (electrical conductivity and permittivity) distribution of a domain is determined by injecting low frequency (typically below 100kHz) AC current and measuring the amplitude and phase of the potentials on electrodes placed on the periphery of the domain. In forward EIT calculations, an estimation of the interior scalar potential field is made given the internal admittivity distribution, under

mixed Neumann and Dirichlet boundary conditions, typically using a finite element discretisation of the domain. The inverse EIT calculation involves estimating an admittivity distribution given the measured amplitude and phase on periphery electrodes.

2.1 The Forward Problem and Jacobian Calculations

In order to solve the inverse admittivity boundary value problem, one requires a forward operator that predicts voltage observations for a given admittivity distribution. For EIT, the forward operator is required to calculate boundary voltages (and the scalar potential distribution for determining the Jacobian, a matrix of partial derivatives), given the current stimuli and an admittivity distribution. For this operator, a mathematical model is derived from Maxwell's equations. Underlying assumptions are that the admittivity is linear and isotropic, and also that the electric and magnetic fields described by Maxwell's equations are slowly varying. The application of the above assumptions to Maxwell's equations results in the derivation of the Laplacian elliptic partial differential equation shown in (1), where γ is the complex admittivity and u is the scalar potential distribution. The forward problem is formulated when (1) is solved (often by finite element discretisation) using a set of boundary conditions, a common choice is the complete electrode model (Somersalo *et al*, 1992).

$$\nabla \bullet (\gamma \nabla u) = 0 \tag{1}$$

A common technique for calculating the admittivity update (the inverse problem) is to approximate the non-linear EIT problem to a linearised problem derived from a Taylor series expansion. Then an iterative admittivity update algorithm can be used to solve the non-linear problem. This method is often referred to as the Gauss-Newton method (if second order terms are neglected). If F is the forward operator that gives $V = F(\gamma)$, the voltages on the electrodes given an admittivity distribution, then a linear approximation is given by (2), where γ_o represents the initial admittivity distribution.

$$F(\gamma) \approx F(\gamma_o) + \frac{\partial F(\gamma_o)}{\partial \gamma_o}(\gamma - \gamma_o) \tag{2}$$

The first derivative, or Jacobian, in (2) can be calculated by the perturbation of power approach (3) (Polydorides, 2002).

$$J_{(d;m,k)} = \frac{\partial V^{(d,m)}}{\partial \gamma_k} = -\iiint_{\Omega_k} \nabla u(I^d) \bullet \nabla u(I^m) dxdydz \tag{3}$$

Where $u(I^d)$ is the potential field created when current is injected and $u(I^m)$ is the potential field that would be created if the measurement electrodes were injecting current. The Jacobian matrix is used in all of the image reconstruction algorithms compared in this paper. A brief description of each algorithm is given in the following section.

2.2 The Inverse Problem

Given the complex vectors $x \in \mathbb{C}^n$ and $b \in \mathbb{C}^m$, and a complex matrix $A \in \mathbb{C}^{m \times n}$, the aim of the inverse problem is to find x, given b and A ($Ax = b$). In the case of EIT, b is the measurement vector, x the admittivity vector and A the Jacobian matrix. Ideally one would solve a system of equations of this type by determining the inverse of the matrix *A*, however, due to its compact nature, it has an unbounded (discontinuous) inverse. This causes A^{-1} to be unstable against variations in the data, hence violating Hadamard's third criterion for well posedness. Several techniques exist for updating the admittivity distribution once the Jacobian matrix has been computed, many using regularisation techniques in order to make the problem less ill-posed.

Perhaps the simplest to implement and one of the most common image reconstruction techniques used in electrical tomography is the back-projection method suggested by Kotre (1989). In Kotre's linear back-projection method, the normalised transpose of the Jacobian is applied to voltage difference data (4), yielding the admittivity update. It can be seen from (4) that Kotre approximated the inverse of the Jacobian matrix with its transpose.

$$d\gamma = J^T dv \tag{4}$$

The Landweber iteration has been adapted for solving the linear inverse problem by Yang *et al* (1999). While the admittivity distribution estimated by the algorithm is far from the true distribution, the residual is dominated by the $J\gamma_n$ term, rather than the noise in the measurement data, v. The Landweber iteration regularises by iteration, with the iteration index being the regularisation parameter. It is important to cease the iterations when the residual becomes comparable to the noise in the measurements (Morozov's discrepancy principle), before the algorithm converges to the unstable least-squares solution. The Landweber algorithm is shown by (5) below, where the relaxation parameter, τ, satisfies $0 < \tau < 2(\| J^T J \|_2)^{-1}$.

$$\gamma_{n+1} = \gamma_n + \tau J^T (v - J\gamma_n) \tag{5}$$

Another technique for solving the EIT inverse problem is the linear conjugate gradients method, a more detailed description of which is provided by Polydorides (2002). The obvious problem of applying a conjugate gradients algorithm to the EIT inverse problem is that the coefficients matrix (Jacobian) is neither square nor positive definite. One solution is to multiply the systems of equations by the transpose of the Jacobian, thus forming a system of normal equations (6). However, a downfall of this formulation is in the calculation of J^TJ, which for large systems is computationally expensive. The system of equations shown in (6) can be readily solved using the MATLAB in-built preconditioned conjugate gradients function. Like the Landweber algorithm, linear conjugate gradients regularise by iteration, and the procedure is controlled by Morozov's discrepancy principle.

$$J^T J\gamma = J^T v \tag{6}$$

An alternative to regularisation by iteration is provided by Tikhonov regularisation, where *a priori* information is incorporated into the algorithm, constraining the solution obtained via the prior information included. A linear Tikhonov regularised Gauss-Newton solution is shown in (7) below.

$$\delta\gamma = (J^T J + \alpha^2 L^T L)^{-1}(J^T \delta v + \alpha^2 L^T L(\gamma_{ref} - \gamma_o)) \tag{7}$$

Where L is a smoothing matrix containing the *a priori* information, α is the regularisation (Tikhonov) parameter and γ_{ref} is an admittivity distribution containing known geometric structures. The use of linear solutions is only valid for small deviations from the admittivity at which the Jacobian is calculated. For large deviations in admittivity, non-linear reconstruction algorithms are required. An example of a non-linear Tikhonov regularised Gauss-Newton solution is shown in (8) below.

$$\gamma_{n+1} = \gamma_n + (J_n^T J_n + \alpha^2 L^T L)^{-1}(J_n^T (v_m - F(\gamma_n)) + \alpha^2 L^T L(\gamma_{ref} - \gamma_n)) \tag{8}$$

A discussion of this family of regularised algorithms has been presented by Lionheart *et al* (2005).

3 Methodology

Experiments were carried out in a 61cm diameter Perspex vessel, filled with mains tap water (conductivity ~0.1 S m^{-1}). The vessel was fitted with four planes of 16, equally spaced, rectangular electrodes of size 6cm^2. The vessel contained four Perspex baffles, 1cm wide and penetrating 6cm into the vessel. The spacing between the electrode planes was 4cm, with a 20cm distance between the base of the vessel and the bottom electrode plane and a 4cm head of water above the top electrode plane. The vessel used is illustrated in Figure 1 below.

Figure 1: The 61cm diameter Perspex vessel used in experiments.

The EIT instrument used for data collection was the University of Manchester/Syngenta LCT2. The LCT2 is capable of injecting current and measuring the amplitude and phase angle of the potential on electrodes in any configuration, up to a present maximum of 64 electrodes. The LCT was chosen for the experiments due to its open architecture, allowing custom measurement strategies and ready access to measurement data. A full description of the LCT2 instrument is provided by York (2005). Measurements were collected using a three-dimensional adjacent strategy. Currents were injected between adjacent electrodes in a plane, starting with the lowest plane and ending with the highest. For each current injection differential measurements were taken between all pairs of adjacent electrodes in each plane. This strategy yields 3904 measurements per measurement frame ("3904" strategy).

Ten repeat measurement frames were taken in order to perform basic statistical analysis, including the calculation of the noise level present in the measurements. The forward problem and Jacobian calculations were performed using the EIDORS-3D toolkit, for further information the reader is referred to Polydorides and Lionheart (2002). Discretisation of the domain (for both the FEM forward problem and the inverse problem) was performed using Netgen, an automatic mesh generator, and the visualisation of results was performed in MayaVi, an open source scientific visualisation package.

4 Image Reconstruction Results

A comparison of the performance of five image reconstruction algorithms described in (4) to (8) will be presented, alongside a typical 3D image reconstruction result obtained from reconstructing a 3D phantom arrangement by making only in-plane voltage measurements. Finally, a reconstruction result obtained using a custom 3D strategy will be presented.

4.1 Reconstruction of a Four Phantom Arrangement

It is common practice in EIT to perform simple rod experiments, using metallic and plastic phantoms, within vessels in order to test image reconstruction algorithms. In this paper, we reconstruct voltage data obtained from the vessel within which four phantoms of various materials of construction and geometry were placed. Figure 2, below, is a schematic of the position of the phantoms within the vessel. The dark phantoms represent plastic rods and the light phantoms metallic rods. Rods positioned approximately half way down the vessel were suspended from vessel furniture by thin plastic coated wire. Figure 3 shows the results of the reconstruction algorithms under examination. Only the real component of the complex admittivity (conductivity) was reconstructed from the data. This was due to the increased computational requirements of conductivity and permittivity imaging and significant noise levels present in the measurement of phase angles caused by uncalibrated measurements (e.g. varying cable lengths).

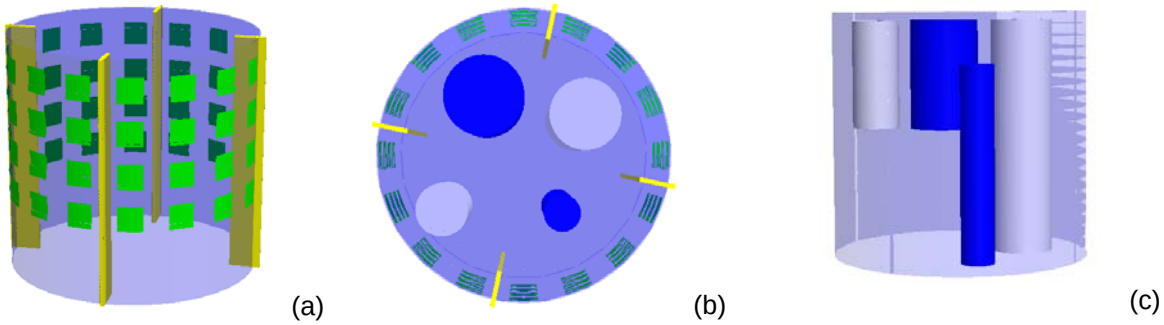

Figure 2: Arrangement of phantoms in the vessel, (a) isometric view showing electrode planes and baffles, (b) plan view illustrating the position of the phantoms, (c) side view illustrating the height of the phantoms. Dark objects are plastic phantoms and light objects are metal phantoms.

Figure 3(a) shows the reconstruction of the measured voltage data by the linear back-projection algorithm (4). The orientation of the image has been selected to give the best view of the phantoms and corresponds, loosely, with that in Figure 2(c). It is clear that the algorithm has reconstructed four phantoms, two plastic and two metal, in approximately the correct spatial positions as indicated by Figure 2. However, the linear back-projection algorithm is not capable of successfully identifying the boundaries of the phantoms, and shifts the phantom positions into the boundary of the domain.

Although still widely used, it is well understood that the normalised transpose of the Jacobian, suggested by Kotre in the linear back-projection algorithm, is a crude approximation to its inverse and the results presented confirm this. Figure 3(b) shows the reconstruction result from the Landweber iteration (5), with a relaxation parameter of $1x10^{-6}$, the algorithm being controlled by Morozov's discrepancy principle. The results from the Landweber algorithm are similar to the linear back-projection algorithm, successfully predicting the approximate spatial positions of the phantoms. However, as with linear back-projection, the Landweber algorithm does not accurately reconstruct the boundaries of the phantoms and over-estimates the diameter of the full-length plastic phantom in the five o'clock position in Figure 2, compared to other algorithms.

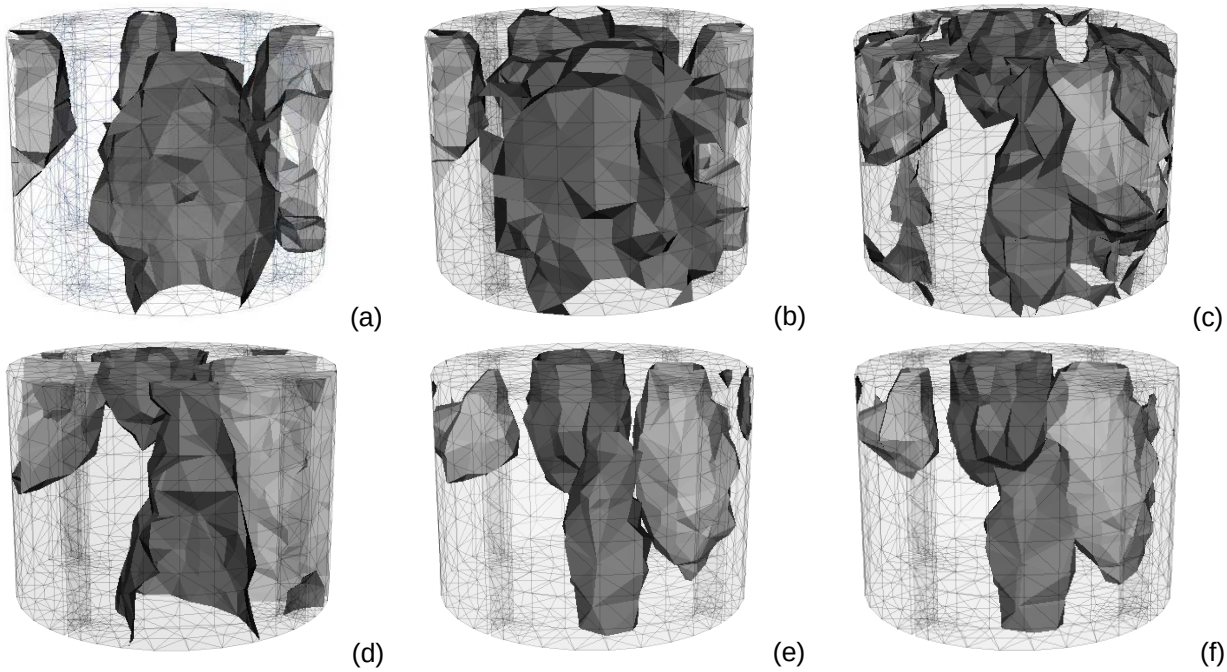

Figure 3: Reconstructed three-dimensional images of the internal conductivity distribution within the vessel for (a) linear back-projection, (b) Landweber, (c) linear regularised Gauss-Newton, (d) non-linear regularised Gauss-Newton, (e) linear conjugate gradients and (f) linear conjugate gradients using only 2D measurements. Dark shading represents less conductive material.

Figure 3(c) shows the conductivity distribution reconstructed by the linear Tikhonov regularised Gauss-Newton algorithm (7). The regularisation parameter used was $1x10^{-6}$ and the regularisation matrix employed was a first-order smoothing operator on the nodes of the finite element mesh. As can be seen in Figure 3(c), the linear Tikhonov regularised algorithm does reconstruct the four phantoms within the vessel. However, the reconstructed conductivity distribution clearly shows artefacts around the top of the vessel and also close to the baffles. Compared to the linear back-projection and Landweber algorithms, the linear Tikhonov regularised algorithm more closely predicts the spatial position and boundaries of the phantoms, but exhibits increased artefacts, especially towards the extremes of the finite element discretisation. The reconstructed conductivity distribution estimated by the non-linear Tikhonov regularised Gauss-Newton algorithm, (8), is presented in Figure 3(d). The regularisation parameter used was $1x10^{-6}$, the maximum number of iterations was 5, and the regularisation matrix employed was a first-order smoothing operator on the nodes of the finite element mesh. Figure 3(d) shows that the non-linear nature of the reconstruction algorithm reduces the artefacts shown by the linear Tikhonov solution. The non-linear Tikhonov solution does predict both the spatial position and boundaries of the phantoms more successfully than the linear back-projection, Landweber and linear Tikhonov solutions. However, when compared to Figure 2, it can be see that the smoothing prior used in the non-linear Tikhonov algorithm does significantly smooth the conductivity distribution. The algorithm predicts the boundaries of the phantoms with limited success, the limitations being caused by attempting to reconstruct a sharp conductivity distribution, whilst using a smoothing prior.

Figure 3(e) shows the reconstructed conductivity distribution predicted by the linear conjugate gradients algorithm (6). This is clearly the most successful algorithm in reconstructing the actual

conductivity profile within the vessel. The success of the linear conjugate gradients algorithm in reconstructing the phantoms is a result of regularising by iteration and not by applying smoothing priors to a non-smooth target distribution. An interesting result is shown by Figure 3(f), where the linear conjugate gradients algorithm was applied to a "2D" measurement strategy. Current injection and voltage measurement are restricted to in-plane electrodes for each of the four planes resulting in 416 measurements ("416" strategy). The performance of the algorithm using 2D measurements is comparable to the performance with 3D measurements. This result comes as a surprise to the authors, as it represents a severely under-determined problem, solving for approximately 5000 unknown conductivity values, using only 416 equations.

Figure 3 illustrates the reconstructed conductivity profiles as 3D isosurfaces, with each surface representing a surface of constant conductivity. This method of presenting 3D results on a 2D medium is, perhaps, the most effective method in conveying the true three-dimensionality of the solution, however, a method for determining the conductivity value of the isosurface is required. One common technique is to take the steepest gradient in conductivity values between adjacent voxels and plot that surface. While this may be a reasonable technique for selecting isosurfaces when the internal distribution is unknown, for the purposes of comparing reconstruction algorithms where the target conductivity profile was known *a priori*, isosurfaces were set at values that most closely represented the target distribution. Figure 4 illustrates the reconstructed conductivity profile from the linear conjugate gradients algorithm, shown as 3D isosurfaces in Figure 3(e), as slices through the vessel. Figure 4 perhaps represents the purest method of displaying reconstruction results, however the images do not have the immediacy of interpretation that 3D isosurfaces offer.

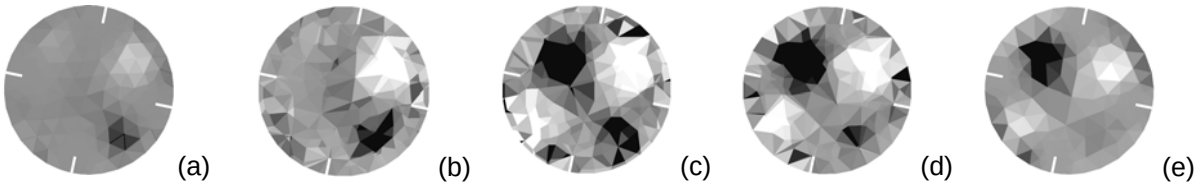

Figure 4: Slice plots showing the reconstructed conductivity distribution within the vessel using linear conjugate gradients at heights of (a) 15cm, (b) 20cm, (c) 40cm, (d) 50cm and (e) 60cm, from the base of the vessel.

The results presented in this paper are only a selection of the results gained from a more widespread comparison of the algorithms with many different phantom arrangements and measurement strategies. Table 1 presents a summary of the algorithm comparison work, where the algorithms are ranked, subjectively, by their ability to reconstruct the target distribution, 1 being the best performer, 5 the worst performer.

Phantom Arrangement	Linear Back Projection	Landweber	Linear Conjugate Gradients	Linear Tikhonov Regularised Gauss-Newton	Non-Linear Tikhonov Regularised Gauss-Newton
Single cylinder	5	4	2	3	1
Multiple cylinders	4	5	1	3	2
Suspended cylinder	4	5	1	3	2

Table 1: Summary of the performance of the reconstruction algorithms using various phantom arrangements.

Table 1 shows that both the non-linear Tikhonov regularised method and the linear conjugate gradients method perform consistently well, with the linear conjugate gradients algorithm out-performing the non-linear Tikhonov method for multiple phantoms, where a sharp conductivity distribution is present in the vessel.

4.2 A Custom Measurement Strategy

The voltage measurements made in the previous section were collected using a 3D adjacent strategy, taking only horizontal differential voltage measurements. Previous work has suggested the

importance of both horizontal and vertical differential voltage measurements for optimum EIT experiments. The measurement strategy employed in data collection for the reconstructed images shown in Figure 5(b) was a 3D opposite strategy, utilising both horizontal and vertical differential voltage measurements. Current was applied between opposite electrodes between two planes at a time (i.e. electrodes 1-25, 2-26, 33-57 etc) current was not driven between non-adjacent electrode planes. Voltage measurements were then made between all non-driving horizontal and vertical electrode pairs on the periphery. This strategy yields 6720 voltage measurements for four planes of 16 electrodes ("6720" strategy). The reconstructed conductivity profile of a flanged plastic cylinder suspended half way down the vessel is shown in Figure 5(b).

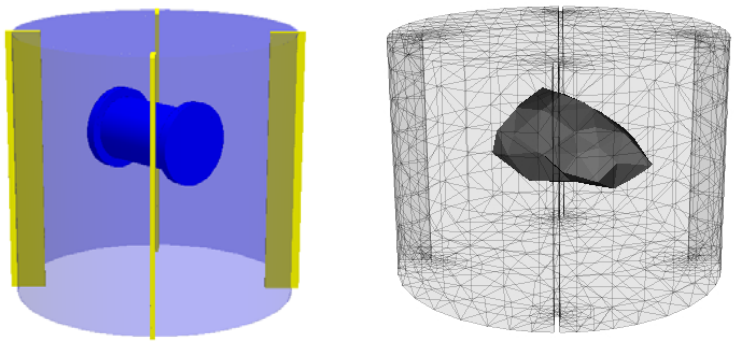

Figure 5: Image reconstruction of a measurement using the ''6720'' strategy, (a) schematic of the position of the phantom within the vessel, (b) reconstructed conductivity distribution using linear conjugate gradients.

The reconstruction algorithm employed was linear conjugate gradients, as the target distribution contained a sharp conductivity distribution. As Figure 5 shows, the combination of the custom measurement strategy and linear conjugate gradients algorithm successfully predict the internal conductivity distribution within the vessel. Attempting to repeat this result using the "416" and "3904" strategies and the linear conjugate gradients algorithm was not successful. The reasons for the success of the "6720" strategy, over the "416" and "3904" strategies, are currently under investigation. It is believed that the "6720" strategy offers increased vertical information not available in the "416" or "3904" strategies. Early results suggest that vertical information is important in reconstructing the type of arrangement shown by Figure 5.

5 Conclusion

The work presented summarises a comparison of 5 common EIT image reconstruction techniques using three-dimensional algorithms and both in-plane and out-of-plane voltage measurements. Results indicate that for the simple situation of high-contrast cylindrical phantoms, the best performing algorithm is linear conjugate gradients. For this arrangement, it is believed that the linear conjugate gradients algorithm performs better than Tikhonov regularised techniques due to sharp boundaries. Smoothing priors currently used in Tikhonov regularisation are more suited to the smooth property profiles more commonly found in industrial processes. It was also found that 2D voltage measurements were comparable to 3D voltage measurements when used in the linear conjugate gradients algorithm. The question "is the extra effort involved in 3D EIT worthwhile?" requires further investigation. Early indications are that for some arrangements, the increased levels of information offered by true 3D EIT are worth the added complexity involved.

Future work in this area will continue to develop improved three-dimensional reconstruction techniques within the EIDORS-3D framework, such as interior point methods for total regularisation, adaptive meshing for increased spatial resolution and customised measurement strategies using singular value decomposition analysis for identifying optimum measurement strategies and reconstruction parameters.

6 References

BORSIC, A. (2002), *Regularization methods for imaging from electrical measurements*, PhD Thesis, Oxford Brookes University, Oxford, UK.

BROWN, B.H. (2001), Medical impedance tomography and process impedance tomography: a brief review*, Meas. Sci. Technol*., 12, pp. 991-996.

CALDERÓN, A.P. (1980), *On an inverse boundary value problem*. In Seminar on Numerical Analysis and Its Applications to Continuum Physics, 67-73, Rio de Janeiro, Sociedade Brasileira de Matematica.

DAILY, W., RAMIREZ, A., LABRECQUE, D. and BINLEY, A., (1995), *Detecting leaks in hydrocarbon storage tanks using electrical resistance tomography*, in Frontiers in Industrial Process Tomography, Eds. SCOTT, D.M, and WILLAIMS, R.A., Engineering Foundation, New York.

DAVIDSON, J.L, RUFFINO, L.S., STEPHENSON, D.R., MANN, R., YORK, T.A. and GRIEVE, B.D (2004). Three-dimensional electrical impedance tomography applied to a metal walled filtration test platform, *Meas. Sci. Technol*., 15, pp. 2263-2274.

DICKIN, F.J., WILLIAMS, R.A. and BECK, M.S., (1993), Determination of composition and motion of multicomponent mixtures in process vessels using electrical impedance tomography –I. Principles and process engineering applications, *Chem. Eng. Sci,* 43, 10, pp. 1883-1897.

DYAKOWSKI, T., JEANMEURE, L.F.C., and JAWORSKI, A.J. (2000), Applications of electrical tomography for gas-solids and liquid-solids flows – a review, *Powder Technology*, 112, pp. 174-192.

KOTRE, C.J., (1989), A sensitivity coefficient method for the reconstruction of electrical impedance tomograms, *Clin. Phys., Physiol. Meas*., 10, pp. 275-281.

LIONHEART, W.R.B., POLYDORIDES, N., and BORSIC, A., (2005), *The Reconstruction Problem*, in, Electrical Impedance Tomography, Methods, History and Applications, Ed. HOLDER, D.S, IOP Series in Medical Physics and Biomedical Engineering, London.

MOLINARI, M., COX, S.J., BLOTT, B.H., and DANIELL, G.J., (2002), Comparison of algorithms for non-linear inverse 3D electrical tomography reconstruction, *Physiol. Meas*. 23, pp. 95-104.

MayaVi scientific visualisation package at http://mayavi.sourceforge.net.

Netgen automatic mesh generator at http://www.hpfem.jku.at.

PINHEIRO, P.A.T., (1998), *A Three-dimensional Image Reconstruction Algorithm for Electrical Resistance Tomography*, PhD Thesis, UMIST, Manchester, UK.

POLYDORIDES, N., (2002), *Image Reconstruction Algorithms for Soft Field Tomography,* PhD Thesis, UMIST, Manchester, UK.

POLYDORIDES, N. and LIONHEART, W.R.B., (2002), A MatLab toolkit for three-dimensional electrical impedance tomography: a contribution to the Electrical Impedance and Diffuse Optical Reconstruction Software project, *Meas. Sci. Technol*., 13, pp. 1871-1883.

SOMERSALO, E., CHENEY, M. and ISAACSON, D., (1992), Existence and uniqueness for electrode models for electric current computed tomography. *SIAM J. Appl. Math.*, 52, pp. 1023-1040.

YANG, W.Q., SPINK, D.M., YORK, T.A. and McCANN, H., (1999), An image reconstruction algorithm based on Landweber's iteration method for electrical capacitance tomography, *Meas. Sci. Technol*., 10, pp. 1065-1069.

YORK, T., MURPHY, S., BURNETT-THOMPSON, A., GRIEVE, B., (2005), *An Accessible Electrical Impedance Imaging System,* In Proc: 4th World Congress on Industrial Process Tomography, Aizu, Japan.